J. Fluid Mech. (2011), *vol.* 671, *pp.* 559–573.
doi:10.1017/S0022112010006051

Boundary-layer thickness effects of the hydrodynamic instability along an impedance wall

SJOERD W. RIENSTRA† AND MIRELA DARAU

Department of Mathematics and Computer Science,
Eindhoven University of Technology, PO Box 513, 5600 MB Eindhoven, The Netherlands

(Received 3 June 2010; revised 9 November 2010; accepted 16 November 2010;
first published online 11 February 2011)

The Ingard–Myers condition, modelling the effect of an impedance wall under a mean flow by assuming a vanishingly thin boundary layer, is known to lead to an ill-posed problem in time domain. By analysing the stability of a linear-then-constant mean flow over a mass-spring-damper liner in a two-dimensional incompressible limit, we show that the flow is absolutely unstable for h smaller than a critical h_c and convectively unstable or stable otherwise. This critical h_c is by nature independent of wavelength or frequency and is a property of liner and mean flow only. An analytical approximation of h_c is given, which is complemented by a contour plot covering all parameter values. For an aeronautically relevant example, h_c is shown to be extremely small, which explains why this instability has never been observed in industrial practice. A systematically regularised boundary condition, to replace the Ingard–Myers condition, is proposed that retains the effects of a finite h, such that the stability of the approximate problem correctly follows the stability of the real problem.

Key words: absolute/convective instability, aeroacoustics, boundary layer stability

1. Introduction

The problem we address is primarily a modelling problem, as we aim to clarify why a seemingly very thin mean flow boundary layer cannot be neglected. At the same time, the physical insight we provide may help to interpret recent experimental results.

Consider a liner of impedance $Z(\omega)$ at a wall along a main flow (U_0, ρ_0, c_0) with boundary layer of thickness h and acoustic waves of typical wavelength λ. At the wall, with vanishing mean flow velocity, the impedance relates the Fourier-transformed pressure $\hat{p}(\omega)$ and normal velocity component $\hat{\boldsymbol{v}}(\omega)\cdot\boldsymbol{n}$ in the following way (see Hubbard 1995):

$$\hat{p} = Z\,(\hat{\boldsymbol{v}}\cdot\boldsymbol{n}) \tag{1.1}$$

(where normal vector $\boldsymbol{n}$ points into the wall). This, however, is not a convenient boundary condition when the mean flow boundary layer is thin and the *effective* mean flow model is one with slip along the wall. In such a case, the Ingard–Myers model (see Ingard 1959; Eversman & Beckemeyer 1972; Tester 1973*b*; Myers 1980)

† Email address for correspondence: s.w.rienstra@tue.nl

utilises the fact that if $h \ll \lambda$, the sound waves do not see any difference between a finite boundary layer and a vortex sheet, so that the limit $h \to 0$ can be taken, resulting into the celebrated Ingard boundary condition (see Ingard 1959) for mean flow along a straight wall in (say) the x-direction:

$$\mathrm{i}\omega(\hat{\boldsymbol{v}} \cdot \boldsymbol{n}) = \left[\mathrm{i}\omega + U_0 \frac{\partial}{\partial x}\right]\left(\frac{\hat{p}}{Z}\right), \tag{1.2}$$

or its generalisation by Myers (1980) for mean flow along a curved wall:

$$\mathrm{i}\omega(\hat{\boldsymbol{v}} \cdot \boldsymbol{n}) = [\mathrm{i}\omega + \boldsymbol{V}_0 \cdot \nabla - \boldsymbol{n} \cdot (\boldsymbol{n} \cdot \nabla \boldsymbol{V}_0)]\left(\frac{\hat{p}}{Z}\right). \tag{1.3}$$

It is clear that both conditions are extremely useful for numerical calculations in those cases in which the boundary layer is indeed negligible.

For a long time, however, there have been doubts (see Tester 1973*a*; Rienstra 2003; Rienstra & Tester 2008) about a particular wave mode that exists along a lined wall with flow and the Ingard–Myers condition. This mode has some similarities with the Kelvin–Helmholtz instability of a free vortex sheet (see Rienstra 2007) and may therefore represent an instability, although the analysis is mathematically subtle (see Brambley & Peake 2006, 2008; Brambley 2008, 2009).

Since there was little or no indication that this instability was genuine, the problem seemed to be of minor practical importance, at least for calculations in frequency domain. However, once we approach the problem in time domain such that numerical errors generate perturbations of every frequency, it appears to our modeller's dislike that the instability is at least in the model very real. The flow appears to be absolutely unstable (see Brambley & Peake 2006; Chevaugeon, Remacle & Gallez 2006) and in fact it is worse: it is ill-posed, as Brambley (2009) has shown. Still, this absolute instability has not (M. G. Jones 2007, personal communication) or at least practically not (see Bauer & Chapkis 1977) been reported in industrial reality, and only very rarely experimentally (see Brandes & Ronneberger 1995; Aurégan, Leroux & Pagneux 2005; Aurégan & Leroux 2008; Marx *et al.* 2009) under special conditions. Although there is little doubt that the limit $h \to 0$ is correct, there must be something wrong in our modelling assumptions. In particular, there must be a very small length scale in the problem, other than λ, on which h scales at the onset of instability. This is what we will consider here.

The present paper consists of three parts. Firstly, we will show that the above modelling anomaly may be explained, in an inviscid model with a vanishingly thin mean shear flow, by the existence of a (non-zero) critical boundary-layer thickness h_c, such that the boundary layer is absolutely unstable for $0 < h < h_c$ and not absolutely unstable (possibly convectively unstable) for $h > h_c$. It appears that for any industrially common configuration, h_c is very small. (We were originally inspired (see Rienstra & Vilenski 2008) for the concept of a critical thickness by the results of Michalke (1965, 1984) for the spatially unstable free shear layer, but it should be noted that an absolute instability is a more complex phenomenon.)

Secondly, we will make an estimate in analytic form of h_c as a function of the problem parameters. This will be valid for a parameter range that includes the industrially interesting cases. A contour plot relating the three dimensionless parameter groups completes the picture for all parameter values.

Thirdly, we will propose a corrected or regularised 'Ingard–Myers' boundary condition, which replaces the boundary layer (like the Ingard–Myers limit) but includes otherwise neglected terms that account for the finite boundary-layer thickness

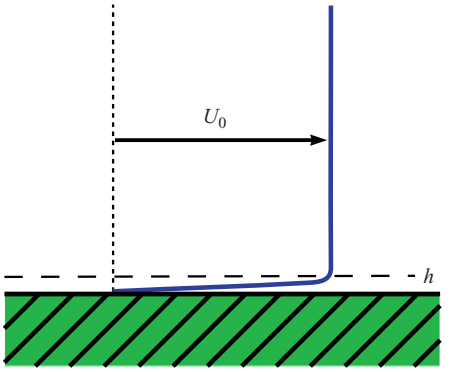

FIGURE 1. (Colour online at journals.cambridge.org/FLM) Mean flow.

effects. This new boundary condition is physically closer to the full problem and predicts (more) correctly stable and unstable behaviour.

2. The problem

2.1. *Description*

An inviscid two-dimensional (2D) parallel mean flow $U_0(y)$ (figure 1), with uniform mean pressure p_0 and density ρ_0, and small isentropic perturbations

$$u = U_0 + \tilde{u}, \quad v = \tilde{v}, \quad p = p_0 + \tilde{p}, \quad \rho = \rho_0 + \tilde{\rho}, \tag{2.1}$$

satisfies the usual linearised Euler equations given by

$$\left.\begin{aligned} \frac{1}{\rho_0 c_0^2}\left(\frac{\partial \tilde{p}}{\partial t} + U_0\frac{\partial \tilde{p}}{\partial x}\right) + \frac{\partial \tilde{u}}{\partial x} + \frac{\partial \tilde{v}}{\partial y} = 0,\\ \frac{\partial \tilde{u}}{\partial t} + U_0\frac{\partial \tilde{u}}{\partial x} + \frac{\mathrm{d}U_0}{\mathrm{d}y}\tilde{v} + \frac{1}{\rho_0}\frac{\partial \tilde{p}}{\partial x} = 0,\\ \frac{\partial \tilde{v}}{\partial t} + U_0\frac{\partial \tilde{v}}{\partial x} + \frac{1}{\rho_0}\frac{\partial \tilde{p}}{\partial y} = 0. \end{aligned}\right\} \tag{2.2}$$

where c_0 is the sound speed and $(\partial_t + U_0\partial_x)(\tilde{p} - c_0^2\tilde{\rho}) = 0$. When we consider waves of the type

$$\tilde{p}(x, y, t) = \frac{1}{2\pi}\int_{-\infty}^{\infty} \breve{p}(x, y; \omega)\,\mathrm{e}^{\mathrm{i}\omega t}\,\mathrm{d}\omega = \frac{1}{4\pi^2}\iint_{-\infty}^{\infty} \hat{p}(y; \alpha, \omega)\,\mathrm{e}^{\mathrm{i}\omega t - \mathrm{i}\alpha x}\,\mathrm{d}\alpha\,\mathrm{d}\omega, \tag{2.3}$$

(similarly for $\tilde{u}$, $\tilde{v}$), the equations become

$$\left.\begin{aligned} \frac{\mathrm{i}(\omega - \alpha U_0)\hat{p}}{\rho_0 c_0^2} - \mathrm{i}\alpha\hat{u} + \frac{\mathrm{d}\hat{v}}{\mathrm{d}y} = 0,\\ \mathrm{i}(\omega - \alpha U_0)\hat{u} + \frac{\mathrm{d}U_0}{\mathrm{d}y}\hat{v} - \frac{\mathrm{i}\alpha}{\rho_0}\hat{p} = 0,\\ \mathrm{i}(\omega - \alpha U_0)\hat{v} + \frac{1}{\rho_0}\frac{\mathrm{d}\hat{p}}{\mathrm{d}y} = 0. \end{aligned}\right\} \tag{2.4}$$

They may be further reduced to a form of the Pridmore-Brown equation (see Pridmore-Brown 1958) by eliminating $\hat{v}$ and $\hat{u}$,

$$\frac{\mathrm{d}^2\hat{p}}{\mathrm{d}y^2} + \frac{2\alpha\dfrac{\mathrm{d}}{\mathrm{d}y}U_0}{\omega-\alpha U_0}\frac{\mathrm{d}\hat{p}}{\mathrm{d}y} + \left(\frac{(\omega-\alpha U_0)^2}{c_0^2} - \alpha^2\right)\hat{p} = 0. \tag{2.5}$$

At $y=0$ we have a uniform impedance boundary condition

$$-\frac{\hat{p}(0)}{\hat{v}(0)} = Z(\omega). \tag{2.6}$$

We select solutions of surface wave type, by assuming exponential decay for $y\to\infty$.

The mean flow is typically uniform everywhere, equal to U_∞, except for a thin boundary layer of thickness h. We look for frequency (ω) and wavenumber (α) combinations that allow a solution. The stability of this solution will be investigated as a function of the problem parameters. In particular, we are interested in the critical thickness $h=h_c$, below which the flow becomes absolutely unstable.

2.2. *Dimensional analysis and scaling*

As the frequency and wavenumber at which the absolute instability first appears are part of the problem, it is clear that h_c does not depend on either ω or α. As a consequence, the Ingard–Myers limit, $h\to 0$, based on $h/\lambda \ll 1$ (λ being a typical acoustic wavelength) is not applicable to the instability problem. Furthermore, since the associated surface wave (see Rienstra 2003, (12)–(13) therein) is of hydrodynamic nature and inherently incompressible, h_c is only weakly depending on sound speed c_0, with p_0 also playing no role any longer. As there are no other length scales in the fluid, h_c must scale on an inherent length scale of the liner. Suppose we have a liner of mass-spring-damper type with resistance R, inertance m and stiffness K, then

$$Z(\omega) = R + \mathrm{i}\omega m - \mathrm{i}K/\omega. \tag{2.7a}$$

If the liner is built from Helmholtz resonators (see Rienstra 2006) of cell depth L and

$$Z(\omega) = R + \mathrm{i}\omega\tilde{m} - \mathrm{i}\rho_0 c_0 \cot(\omega L/c_0), \tag{2.7b}$$

and designed to work near the first cell resonance frequency (where $\mathrm{Im}(Z)=0$), then $\omega L/c_0$ is small for the relevant frequency range, and we can approximate the Helmholtz resonator by a mass-spring-damper system with $K\simeq\rho_0 c_0^2/L$ and $m=\tilde{m}+\frac{1}{3}\rho_0 L$ (see Richter 2009). Thus, we have six parameters (h_c, ρ_0, U_∞, R, m, K) and three dimensions (m, kg, s), so it follows from Buckingham's theorem that our problem has three dimensionless numbers, for example

$$\frac{R}{\rho_0 U_\infty}, \quad \frac{mK}{\rho_0^2 U_\infty^2}, \quad \frac{Kh_c}{\rho_0 U_\infty^2}. \tag{2.8}$$

In § 3.3, we will see that a proper reference length scale for h_c, i.e. one that preserves its order of magnitude, is a more complicated combination of these parameters. More specifically, we will find that we can write, for a function $H=O(1)$,

$$h_c = \left(\frac{\rho_0 U_\infty}{R}\right)^2 U_\infty\sqrt{\frac{m}{K}}\,H\left(\frac{R}{\rho_0 U_\infty}, \frac{\sqrt{mK}}{\rho_0 U_\infty}\right). \tag{2.9}$$

However, at this stage, nothing can be said about this scaling. Since non-dimensionalisation on arbitrary scaling values is not particularly useful, at least not here, we therefore deliberately leave the problem in *dimensional* form.

2.3. *The model: incompressible linear-then-constant shear flow*

As the stability problem is essentially incompressible, we consider the incompressible limit, where $\omega/\alpha, U_0 \ll c_0$. Then, the Pridmore-Brown equation reduces to

$$\frac{\mathrm{d}^2\hat{p}}{\mathrm{d}y^2} + \frac{2\alpha\dfrac{\mathrm{d}}{\mathrm{d}y}U_0}{\omega - \alpha U_0}\frac{\mathrm{d}\hat{p}}{\mathrm{d}y} - \alpha^2\hat{p} = 0. \tag{2.10}$$

If we assume a linear-then-constant velocity profile of thickness h,

$$U_0(y) = \begin{cases} \dfrac{y}{h}U_\infty, & \text{for} \quad 0 \leqslant y \leqslant h, \\ U_\infty, & \text{for} \quad h \leqslant y < \infty, \end{cases} \tag{2.11}$$

we have an exact solution for our problem. For $y \geqslant h$, we have

$$\hat{p} = A\,\mathrm{e}^{-|\alpha|y}, \quad \text{where } |\alpha| = \operatorname{sgn}(\operatorname{Re}\alpha)\alpha. \tag{2.12}$$

Other representations of $|\alpha|$ are $\sqrt{\alpha^2}$ or $\sqrt{\mathrm{i}\alpha}\sqrt{-\mathrm{i}\alpha}$ with principal square roots assumed for $\sqrt{\cdot}$ in all cases. Note that $|\alpha|$ is the generalisation of the real absolute value function which is analytic in the right and the left complex half-planes. It has discontinuities along $(-\mathrm{i}\infty, 0)$ and $(0, \mathrm{i}\infty)$, which correspond with the branch cuts of the square roots. The notation $|\alpha|$ is very common in this kind of problems (see Peake 1997, 2002; Lingwood & Peake 1999), but of course should not be confused with the complex modulus of α. However, in this paper the complex modulus does not occur.

In the shear layer region $(0, h)$, we have

$$\hat{p}(y) = C_1\,\mathrm{e}^{\alpha y}(h\omega - \alpha y U_\infty + U_\infty) + C_2\,\mathrm{e}^{-\alpha y}(h\omega - \alpha y U_\infty - U_\infty), \tag{2.13a}$$

$$\hat{u}(y) = \frac{\alpha h}{\rho_0}(C_1\,\mathrm{e}^{\alpha y} + C_2\,\mathrm{e}^{-\alpha y}), \tag{2.13b}$$

$$\hat{v}(y) = \frac{\mathrm{i}\alpha h}{\rho_0}(C_1\,\mathrm{e}^{\alpha y} - C_2\,\mathrm{e}^{-\alpha y}). \tag{2.13c}$$

This last solution is due to Rayleigh (see Drazin & Reid 2004), but has been used in a similar context of stability of flow along a flexible wall by Lingwood & Peake (1999).

2.4. *The dispersion relation*

When we apply continuity of pressure and particle displacement (which is, in this case, equivalent to continuity of normal velocity, since the mean flow is continuous) at the interface $y = h$, and the impedance boundary condition at $y = 0$, we obtain the necessary relation between ω and α for a solution to exist. This is the dispersion relation of the waves of interest, given by

$$0 = D(\alpha, \omega) = Z(\omega) + \frac{\mathrm{i}\rho_0}{\alpha h}\frac{(h\omega - U_\infty)(\alpha h\Omega + |\alpha|(h\Omega + U_\infty))\,\mathrm{e}^{\alpha h} + (h\omega + U_\infty)(\alpha h\Omega - |\alpha|(h\Omega - U_\infty))\,\mathrm{e}^{-\alpha h}}{(\alpha h\Omega + |\alpha|(h\Omega + U_\infty))\,\mathrm{e}^{\alpha h} - (\alpha h\Omega - |\alpha|(h\Omega - U_\infty))\,\mathrm{e}^{-\alpha h}}, \tag{2.14}$$

where

$$\Omega = \omega - \alpha U_\infty. \tag{2.15}$$

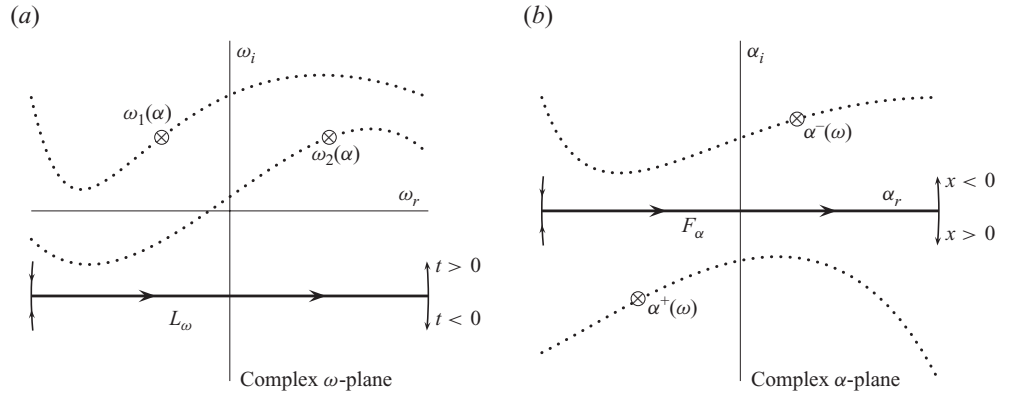

FIGURE 2. Paths of integration in (*a*) the ω-plane and (*b*) the α-plane between *sketched* possible behaviour of poles.

3. Stability analysis

3.1. *Briggs–Bers analysis*

We are essentially interested in any possible *spurious* absolutely unstable behaviour of our model, as this has by far the most dramatic consequences for numerical calculation in time domain (see Chevaugeon *et al.* 2006). Of course, it is also of interest if the instability is physically genuine, as may be the case in the papers of Brandes & Ronneberger (1995), Aurégan *et al.* (2005), Aurégan & Leroux (2008) and Marx *et al.* (2009), but for aeronautical applications this is apparently very rare (see Bauer & Chapkis 1977; M. G. Jones 2007, personal communication).

To identify an absolutely unstable behaviour, we have to search for causal modes with vanishing group velocity (and an additional 'pinching' requirement). For this, we follow the method originally developed by Briggs (1964) and Bers (1983) for plasma physics applications, but subsequently widely applied for fluid mechanical and aeroacoustical applications (see Huerre & Monkewitz 1985; Peake 1997; Lingwood & Peake 1999; Peake 2002; Brambley & Peake 2006, 2008).

If the impulse response of the system is represented generically by a double Fourier integral

$$\Psi(x, y, t) = \frac{1}{(2\pi)^2} \int_{L_\omega} \int_{F_\alpha} \frac{\varphi(y)}{D(\alpha, \omega)} \, \mathrm{e}^{\mathrm{i}\omega t - \mathrm{i}\alpha x} \, \mathrm{d}\alpha \, \mathrm{d}\omega, \tag{3.1}$$

the integration contours L_ω and F_α (figure 2) have to be located in domains of *absolute convergence* in the complex ω- and α-planes as follows.

(i) For the ω-integral, L_ω should be below any poles $\omega_j(\alpha)$ given by $D(\alpha, \omega) = 0$, where $\alpha \in F_\alpha$. This is due to causality that requires $\Psi = 0$ for $t < 0$ and the $\mathrm{e}^{\mathrm{i}\omega t}$-factor.

(ii) For the α-integral, F_α should be in a strip along the real axis between the left and right running poles, $\alpha^-(\omega)$ and $\alpha^+(\omega)$ given by $D(\alpha, \omega) = 0$, for $\omega \in L_\omega$.

The main idea is that we exploit the freedom we have in the location of L_ω and F_α. As a first step, we check that there exists a minimum imaginary part of the possible ω_j:

$$\omega_{min} = \min_{\alpha \in \mathbb{R}} [\mathrm{Im}\, \omega_j(\alpha)]. \tag{3.2}$$

This is relatively easy for a mass-spring-damper impedance, because the dispersion relation is equivalent to a third-order polynomial in ω with just three solutions, which can be traced without difficulty. See figure 3 for a typical case (note that it suffices

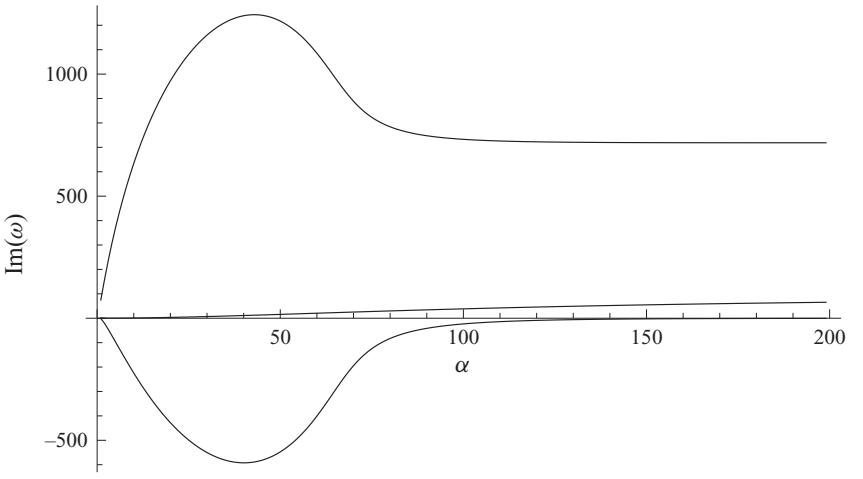

FIGURE 3. Plots of $\mathrm{Im}(\omega_j(\alpha))$ for $\alpha \in \mathbb{R}$. All have a minimum imaginary part, so the Briggs–Bers method is applicable ($\rho_0 = 1.22$, $U_\infty = 82$, $h = 0.01$, $R = 100$, $m = 0.1215$, $K = 8166$).

to consider $\mathrm{Re}(\alpha) > 0$ because of the symmetry of D). There is a minimum imaginary part, so Briggs–Bers' method is applicable. Since $\omega_{min} < 0$, the flow is unstable.

Then, we consider poles α^+ and α^- in the α-plane, and plot $\alpha^{\pm}(\omega)$-images of the line $\mathrm{Im}(\omega) = c \geqslant \omega_{min}$. Note that while c is increased, the contour F_α has to be deformed in order not to cross the poles, but always via the origin because of the branch cuts along the imaginary axis. As c is increased, α^+ and α^- approach each other until they collide for $\omega = \omega^*$ into $\alpha = \alpha^*$, where the F_α-integration contour is pinched, unable to be further deformed; see figure 4 for a typical case. If $\mathrm{Im}(\omega^*) < 0$, respectively >0, then (ω^*, α^*) corresponds to an absolute, respectively convective, instability. Since two solutions of $D(\alpha, \omega) = 0$ coalesce, they satisfy the additional equation $(\partial/\partial\alpha)D(\alpha, \omega) = 0$, so (ω^*, α^*) must satisfy the two equations and, in addition, it must be the collision of a right- and a left-running mode (this can be checked on the plots in the α-plane).

3.2. *A typical example from aeronautical applications*

As a typical aeronautical example, we consider a low-Mach-number mean flow $U_\infty = 60\,\mathrm{m\,s^{-1}}$, $\rho_0 = 1.225\,\mathrm{kg\,m^{-3}}$ and $c_0 = 340\,\mathrm{m\,s^{-1}}$, with an impedance of the Helmholtz resonator type (see Rienstra 2006)

$$Z(\omega) = R + \mathrm{i}\omega\tilde{m} - \mathrm{i}\rho_0 c_0 \cot\left(\frac{\omega L}{c_0}\right) \approx R + \mathrm{i}\omega\left(\tilde{m} + \frac{1}{3}\rho_0 L\right) - \mathrm{i}\frac{\rho_0 c_0^2}{\omega L}, \tag{3.3}$$

which is chosen such that $R = 2\rho_0 c_0 = 833\,\mathrm{kg\,(m^2\,s)^{-1}}$, cell depth $L = 3.5\,\mathrm{cm}$ and $\tilde{m}/\rho_0 = 20\,\mathrm{mm}$, leading to $K = 4.0 \times 10^6\,\mathrm{kg\,(m^2\,s^2)^{-1}}$ and $m = 0.039\,\mathrm{kg\,m^{-2}}$.

When we vary the boundary-layer thickness h, and plot the imaginary part (=minus growth rate) of the found frequency ω^*, we see that once h is small enough, the instability becomes absolute (see figure 5). We call the value of h where $\mathrm{Im}(\omega^*) = 0$ the critical thickness h_c, because for any $h < h_c$ the instability is absolute. Note that $\mathrm{Im}(\omega^*) \to -\infty$ for $h \downarrow 0$ so the growth rate becomes unbounded for $h = 0$, which confirms the ill-posedness of the Ingard–Myers limit, as observed by Brambley (2009). For the present example, the critical thickness h_c appears to be extremely

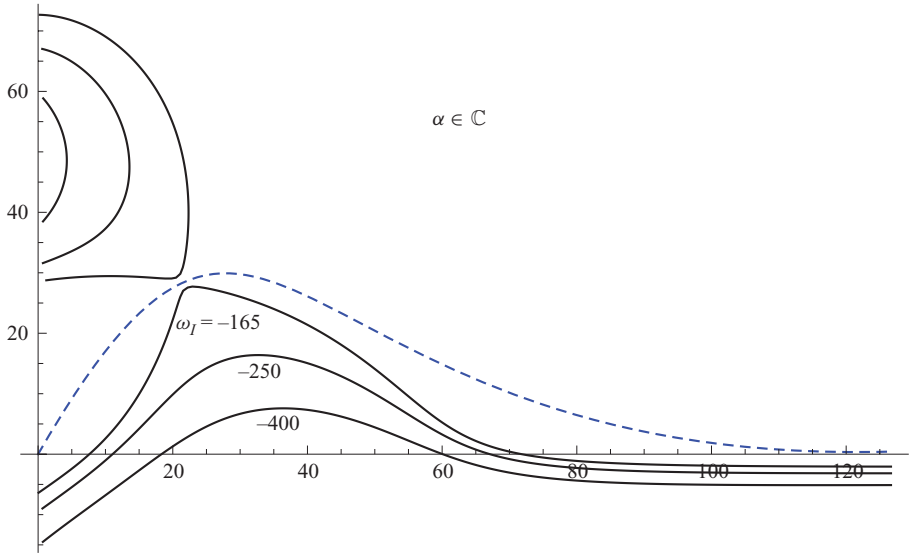

FIGURE 4. (Colour online) Plots of poles $\alpha^+(\omega)$ and $\alpha^-(\omega)$ for varying $\mathrm{Im}(\omega) = c$ until they collide for $c = -165$. Therefore, in this example (with $\rho_0 = 1.22$, $U_\infty = 82$, $h = 0.01$, $R = 100$, $m = 0.1215$, $K = 8166$), the flow is absolutely unstable. The dashed line is the deformed integration contour F_α.

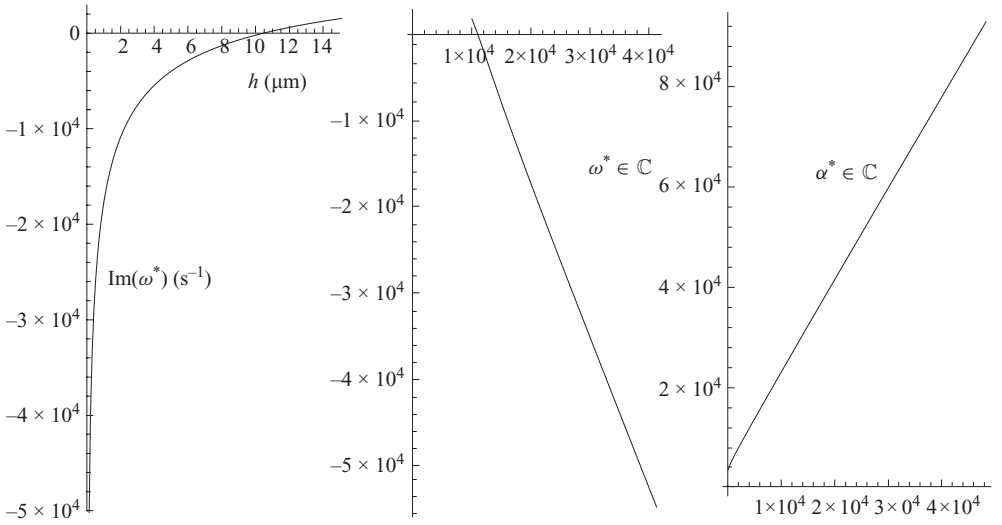

FIGURE 5. Growth rate $\mathrm{Im}(\omega^*)$ against h of potential absolute instability at vanishing group velocity (pinch point) is plotted together with the corresponding complex frequency ω^* and wavenumber α^*.

small, namely

$$h_c = 10.5 \times 10^{-6}\,\mathrm{m} = 10.5\,\mu\mathrm{m}, \text{ with } \omega^* = 11023.4\,\mathrm{s}^{-1},\ \alpha^* = 364.887 + \mathrm{i}4188.99\,\mathrm{m}^{-1}. \tag{3.4}$$

This result is typical. For other industrially relevant liner top plate porosities and thicknesses (leading to other values of $\tilde{m}$), we find similar values, namely $h_c = 8.5\,\mu\mathrm{m}$ for $\tilde{m}/\rho_0 = 10\,\mathrm{mm}$, and $h_c = 13.6\,\mu\mathrm{m}$ for $\tilde{m}/\rho_0 = 40\,\mathrm{mm}$.

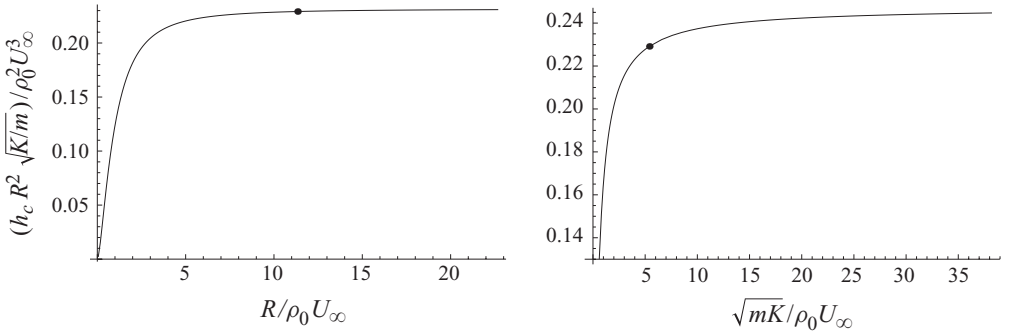

FIGURE 6. Variation in R and $\sqrt{mK}$ with $U_\infty = 60$, $\rho_0 = 1.225$, $K = 4 \times 10^6$, $R = 2\rho_0 c_0$ and $m = 0.039$. The dot corresponds to the conditions of the example in § 3.2.

It is clear that these values are smaller than any practical boundary-layer thickness, so a real flow will not be absolutely unstable, in contrast to any model that adopts the Ingard–Myers limit, even though this is at first sight a very reasonable assumption if the boundary layer is only a fraction of any relevant acoustic wavelength.

3.3. *Approximation for large $R/\rho_0 U_\infty$ and large $\sqrt{mK}/R$*

Insight is gained into the functional relationship between h_c and the other problem parameters by considering relevant asymptotic behaviour. If the wall has a high 'hydrodynamic' resistance, i.e. $r = R/\rho_0 U_\infty \gg 1$, and a high quality factor of the resonator, i.e. $\sqrt{mK}/R = O(r)$, then the inherent scalings for h_c appear to be $m/\rho_0 h_c = O(r^4)$, $\alpha h_c = O(r^{-1})$ and $\omega h_c/U_\infty = O(r^{-2})$, such that we get to leading order from $D(\alpha, \omega) = 0$ and $D_\alpha(\alpha, \omega) = 0$:

$$\left.\begin{aligned} \mathrm{i}\left(m\omega - \frac{K}{\omega}\right) + \left(R + \mathrm{i}\rho_0 U_\infty \frac{\alpha h_c}{\dfrac{\omega h_c}{U_\infty} - \alpha^2 h_c^2}\right) + \cdots = 0, \\ \left(\frac{\mathrm{i}}{\dfrac{\omega h_c}{U_\infty} - \alpha^2 h_c^2} + \frac{2\mathrm{i}\alpha^2 h_c^2}{\left(\dfrac{\omega h_c}{U_\infty} - \alpha^2 h_c^2\right)^2}\right) + \cdots = 0. \end{aligned}\right\} \tag{3.5}$$

With the condition that ω is real, we have

$$\omega \simeq \sqrt{\frac{K}{m}}, \quad \frac{\omega h_c}{U_\infty} + (\alpha h_c)^2 \simeq 0, \quad \frac{R}{\rho_0 U_\infty} - \frac{\mathrm{i}}{2\alpha h_c} \simeq 0, \tag{3.6}$$

resulting into the approximate relation

$$h_c \simeq \frac{1}{4}\left(\frac{\rho_0 U_\infty}{R}\right)^2 U_\infty \sqrt{\frac{m}{K}}. \tag{3.7}$$

This is confirmed by the numerical results given in figures 6 and 7. Here, dimensionless quantity

$$\frac{h_c R^2 \sqrt{K/m}}{\rho_0^2 U_\infty^3} = H\left(\frac{R}{\rho_0 U_\infty}, \frac{\sqrt{mK}}{\rho_0 U_\infty}\right) \tag{3.8}$$

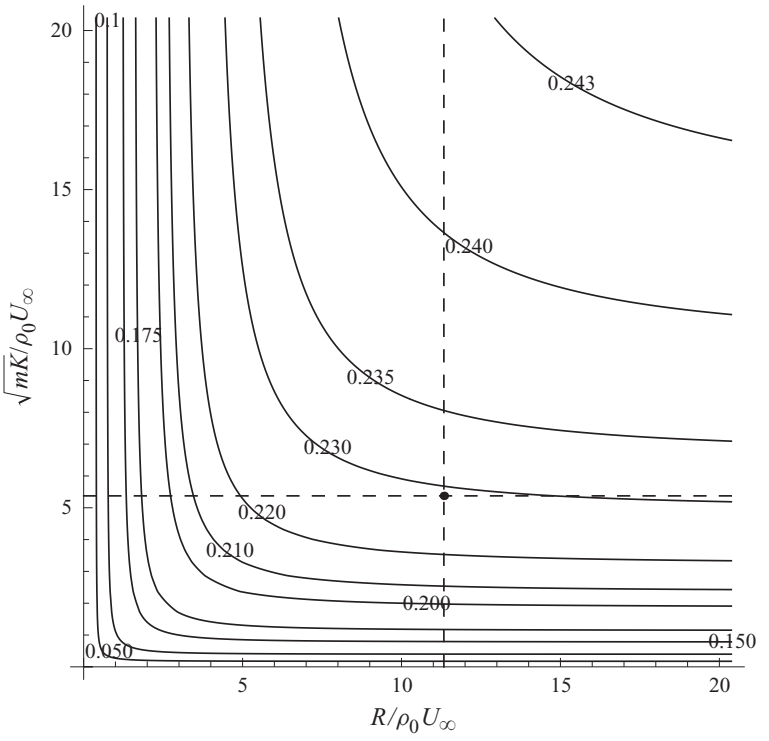

FIGURE 7. Contour plot of $h_c R^2 \sqrt{K/m}/(\rho_0^2 U_\infty^3)$ as a function of $R/\rho_0 U_\infty$ and $\sqrt{mK}/\rho_0 U_\infty$. The dashed lines correspond to figure 6. The dot corresponds to the conditions of the example in § 3.2.

(the function H of (2.9)) is plotted as a function of dimensionless parameters $R/\rho_0 U_\infty$ and $\sqrt{mK}/\rho_0 U_\infty$. In figure 6, one parameter is varied while the other is held fixed at the conditions of the example in § 3.2 and vice versa. An even more comprehensive result is given in figure 7, where a contour plot of H is given. From (3.7) we know that H becomes asymptotically equal to 0.25. Indeed, we see that for a rather large parameter range, including the above example (indicated by a dot), H is found between 0.2 and 0.25. Therefore, expression (3.7) appears to be a good estimate of h_c for R, K and m not too close to zero.

4. A regularised boundary condition

4.1. *Approximations for small* αh

If we carefully consider the *third*-order approximations of the exponentials for $\alpha h \to 0$, i.e. $\mathrm{e}^{\pm\alpha h} \simeq 1 \pm \alpha h + \frac{1}{2}(\alpha h)^2 \pm \frac{1}{6}(\alpha h)^3$, of both the numerator and denominator of the dispersion relation $D(\alpha, \omega) = 0$, then collect powers of αh up to $O(\alpha h)$, with $\omega h/U_\infty = O(\alpha h)$, and ignore higher-order terms, we find

$$Z(\omega) \simeq \frac{\rho_0}{\mathrm{i}} \frac{\Omega^2 + |\alpha| \left(\omega\Omega + \frac{1}{3} U_\infty^2 \alpha^2 \right) h}{|\alpha|\omega + \alpha^2 \Omega h}, \tag{4.1}$$

where $\Omega = \omega - \alpha U_\infty$. This expansion is obviously not unique. We can multiply numerator and denominator by any suitable function of αh, re-expand and obtain

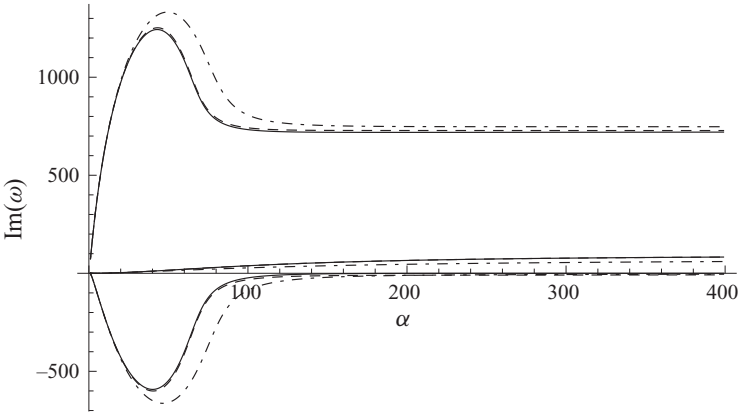

FIGURE 8. Plots of $\mathrm{Im}(\omega_j(\alpha))$ for $\alpha \in \mathbb{R}$ for the exact (solid) and the approximate ($\theta = \frac{1}{3}$, dashed; $\theta = 0$, dot-dashed) dispersion relation. The parameter values are the same as in figure 3.

a different, but asymptotically equivalent form. For example, we can multiply by $\mathrm{e}^{-|\alpha|h\theta}/\mathrm{e}^{-|\alpha|h\theta}$ and obtain after re-expanding the numerator and denominator

$$Z(\omega) \simeq \frac{\rho_0}{\mathrm{i}} \frac{\Omega^2 + |\alpha|\left((1-\theta)\omega^2 - (1-2\theta)\omega\alpha U_\infty + \left(\frac{1}{3} - \theta\right)\alpha^2 U_\infty^2\right)h}{|\alpha|\omega + \alpha^2(\Omega - \theta\omega)h}. \tag{4.2}$$

It is not immediately clear if there is a practically preferable choice of θ, but a particularly pleasing result seems to be obtained by $\theta = \frac{1}{3}$. For this choice, the coefficient of the highest power of α in the numerator is reduced to 2 and the approximate solutions are remarkably close to the 'exact' ones, at least in the industrial example considered here, as shown below (§4.3, figure 8). Therefore, in the following, we will continue with the approximation

$$Z(\omega) \simeq \frac{\rho_0}{\mathrm{i}} \frac{\Omega^2 + |\alpha|\omega\left(\frac{2}{3}\omega - \frac{1}{3}\alpha U_\infty\right)h}{|\alpha|\omega + \alpha^2\left(\Omega - \frac{1}{3}\omega\right)h} = \frac{\mathrm{i}\Omega - \rho_0 \frac{-|\alpha|}{\mathrm{i}\Omega\rho_0}\mathrm{i}\omega\left(\frac{2}{3}\mathrm{i}\omega - \frac{1}{3}\mathrm{i}\alpha U_\infty\right)h}{\mathrm{i}\omega\frac{-|\alpha|}{\mathrm{i}\Omega\rho_0} + \frac{(-\mathrm{i}\alpha)^2}{\rho_0}h - \frac{1}{3}\mathrm{i}\omega\frac{-|\alpha|}{\mathrm{i}\Omega\rho_0}|\alpha|h}, \tag{4.3}$$

recast in a form convenient later.

4.2. *A modified Ingard–Myers boundary condition*

Although the approximation is for small αh, it should be noted that the behaviour for large α is such that the solutions of *this* approximate dispersion relation have exactly the same behaviour with respect to the stability as the solutions of the original $D(\alpha, \omega) = 0$ (see below). Not only are all modes $\omega_j(\alpha)$ bounded from below when $\alpha \in \mathbb{R}$, but also h_c as a function of the problem parameters is found very similar to the 'exact' one for the practical cases considered above. It therefore makes sense to consider an equivalent boundary condition that exactly produces this approximate dispersion relation and hence replaces the effect of the boundary layer (just like the Ingard–Myers limit) but now with a *finite* h. If we include a small but non-zero h, the ill-posedness and the associated absolute instability can be avoided.

Most importantly, this is without sacrificing the physics but, on the contrary, by restoring a little bit of the inadvertently neglected physics.

If we identify at $y=0$,

$$-\mathrm{i}\alpha\hat{p} \sim \frac{\partial}{\partial x}\check{p}, \quad \frac{-|\alpha|}{\mathrm{i}\Omega\rho_0}\hat{p} = (\hat{\boldsymbol{v}}\cdot\boldsymbol{n}), \quad |\alpha|(\hat{\boldsymbol{v}}\cdot\boldsymbol{n}) \sim \frac{\partial}{\partial \boldsymbol{n}}(\check{\boldsymbol{v}}\cdot\boldsymbol{n}), \tag{4.4}$$

for the normal vector $\boldsymbol{n}$ pointing *into* the surface, then we have a 'corrected' or 'regularised' Ingard–Myers boundary condition

$$Z(\omega) = \frac{\left(\mathrm{i}\omega + U_\infty\dfrac{\partial}{\partial x}\right)\check{p} - h\rho_0\mathrm{i}\omega\left(\dfrac{2}{3}\mathrm{i}\omega + \dfrac{1}{3}U_\infty\dfrac{\partial}{\partial x}\right)(\check{\boldsymbol{v}}\cdot\boldsymbol{n})}{\mathrm{i}\omega(\check{\boldsymbol{v}}\cdot\boldsymbol{n}) + \dfrac{h}{\rho_0}\dfrac{\partial^2}{\partial x^2}\check{p} - \dfrac{1}{3}h\mathrm{i}\omega\dfrac{\partial}{\partial \boldsymbol{n}}(\check{\boldsymbol{v}}\cdot\boldsymbol{n})}, \tag{4.5}$$

which indeed reduces for $h=0$ to the Ingard approximation, but now has the *physically correct* stability behaviour. (Note that the Myers generalisation for curved surfaces is far more complicated.)

Recently, Brambley (2010) proposed a corrected Ingard boundary condition for cylindrical duct modes and smooth velocity profiles of compressible flows, derived from an approximate solution of matched expansion type for thin mean flow boundary layers, similar to the solution by Eversman & Beckemeyer (1972). At first sight, his results, when applied to a linear-then-constant profile, are not exactly in agreement with (4.1), but, as we pointed out before, these approximations are not unique, and, to the best of our knowledge, Brambley's and our forms are asymptotically equivalent (apart from an obvious 2D–3D difference). In particular, there is no difference due to compressibility effects because these are of higher order in αh.

4.3. *Stability behaviour of the approximate dispersion relation*

A way to study the well-posedness of the problem with the regularised boundary condition for a mass-spring-damper impedance is to verify the lower boundedness of $\mathrm{Im}(\omega)$ as a function of α. Since ω is continuous in α and finite everywhere, it is enough to consider the asymptotic behaviour to large real α while keeping the other length scales fixed. Equation (4.3) leads to a third-order polynomial in ω. Using perturbation techniques for small $1/\alpha$, we find that two of the roots behave to leading order as

$$\omega = \mathrm{i}\frac{R}{2m} \pm \mathrm{i}\frac{1}{2m}\sqrt{R^2 - 4Km} + O(1/\alpha), \tag{4.6}$$

while the third one is given by

$$\omega = \frac{3}{2}\alpha U_\infty - \mathrm{sgn}(\alpha)\left(\frac{9}{4} + \frac{\rho_0 h}{m}\right)\frac{U_\infty}{h} + O(1/\alpha). \tag{4.7}$$

Therefore, for two of the three solutions, the imaginary part of ω tends to some constant values, while the third is $O(1/\alpha)$ and so approaches zero. This is confirmed by figure 8 for the same parameter values as in figure 3. Such being the case, the Briggs–Bers method is applicable.

If, for the proposed boundary condition (4.5), we vary again h and plot for the example of § 3.2 (as in figure 5), the imaginary part of the frequency ω^*, with $\mathrm{Im}(\omega^*)=0$, we find practically the same results as for the 'exact value' (figure 9). Also, the value h_c for which the flow turns from convectively unstable to absolutely unstable is very close to the 'exact' value.

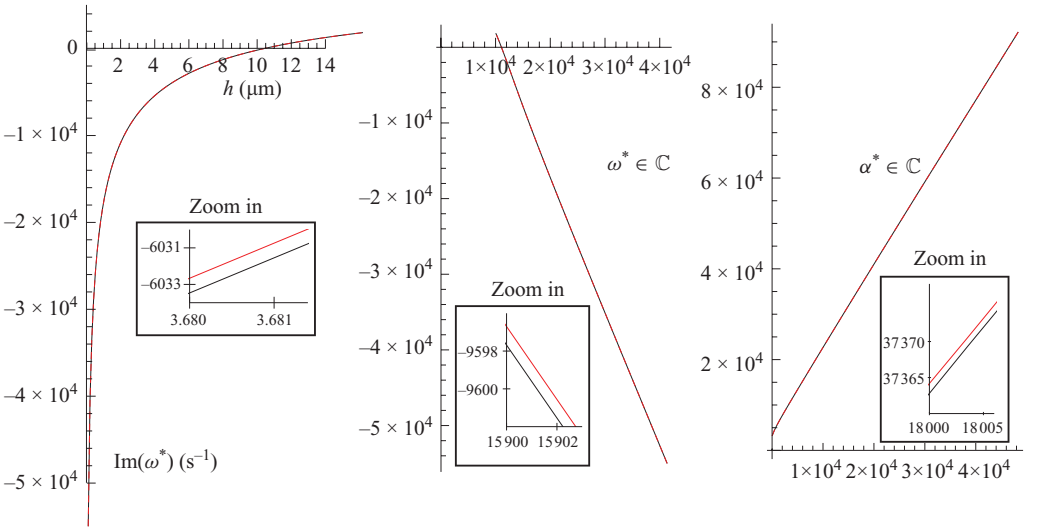

FIGURE 9. (Colour online) Comparison for the exact (solid) with approximate (dashed) solution using (4.5): growth rate $\mathrm{Im}(\omega^*)$ against h of potential absolute instability at vanishing group velocity (pinch point) is plotted together with the corresponding complex frequency ω^* and wavenumber α^*.

A rather good agreement was also found for the approximation that corresponds with $\theta = 0$ (4.1) but the present high accuracy is definitely due to the particular choice of $\theta = \frac{1}{3}$ (4.3). See for example figure 8, where exact results are compared with the approximations for $\theta = 0$ and $\theta = \frac{1}{3}$. A similar comparison in figure 9 is not given although it would have led to the same conclusion. The typical error $O(10^2)$ of the $\theta = 0$ approximation would be too small for the large graphs, but too big for the zoom-ins, to be visible.

From these results, we think it is reasonable to assume that the stability behaviour of the regularised Ingard–Myers boundary condition is the same for the industrially relevant cases as for the finite boundary-layer model studied here.

5. Conclusions

The stability of a mass-spring-damper liner with incompressible flow with linear-then-constant velocity profile has been analysed. The flow is found to be absolutely unstable for small but finite boundary layer h, say $0 < h < h_c$. In the limit of $h \downarrow 0$, the growth rate tends to infinity and the flow may be called *hyper-unstable*, which confirms the ill-posedness of the Ingard–Myers limit. These results in the incompressible assumption are confirmed in the recent paper by Brambley (2010) for compressible flows.

The critical thickness h_c is a property of flow and liner, and has no relation with any acoustic wavelength. Therefore, neglecting the effect of a finite h (as is done when applying the Ingard–Myers limit) cannot be justified by comparing h with a typical acoustic wavelength. An explicit approximate formula for h_c is formulated, which incidentally shows that the characteristic length scale for h_c is not easily guessed from the problem. This analytic result is completed by a contour plot giving h_c for all parameter values. Anticipating a weak dependence of h_c on Mach number and geometry, this result could be very useful for numerical simulations, to assess the order of magnitude of boundary layers that are not absolutely unstable.

In industrial practice, h_c is much smaller than any prevailing boundary-layer thicknesses, which explains why the absolute instability of the present kind has not yet been observed. Although apparently never observed in industrial practice, there may be a convective instability that remains too small to be measured (in all the examples we investigated we found for $h > h_c$ a convective instability). The fact that we found no stable cases may be due to the simplifications adopted for our model.

The very existence of this critical h_c emphasises that $h = 0$ is not an admissible modelling assumption, and a proper model (at least in time domain) will have to have a finite $h > h_c$ in some way. Therefore, a corrected 'Ingard–Myers' condition, including h, is proposed, which is not absolutely unstable for $h > h_c$. Since this is based on a 2D incompressible model with a linear velocity profile, it goes without saying that some margin is to be taken when applied in a more realistic situation.

The linear profile has the great advantage of an exact solution, but of course the price to be paid is the absence of a critical layer singularity (see Campos, Oliveira & Kobayashi 1999), i.e. a singularity of the solution at $y = y_c$, where $\omega - \alpha U_0(y_c) = 0$. This is subject of ongoing research.

This paper is an adapted and extended version of the IUTAM 2010 Symposium on Computational Aero-Acoustics contribution (see Rienstra & Darau 2010).

We gratefully acknowledge that the present project is a result of the cooperation between the Eindhoven University of Technology (Netherlands), Department of Mathematics and Computer Science, and the West University of Timisoara (Romania), Faculty of Mathematics and Informatics, realised, supervised and guided by professors Robert R. M. Mattheij and Stefan Balint.

We thank professor Patrick Huerre for his advice and helpful suggestions on the stability analysis. We thank Thomas Nodé-Langlois, Michael Jones, Edward Rademaker and Andrew Kempton for their help with choosing typical liner parameters. We also thank Ed Brambley for noting the apparent difference between his approximate dispersion relation and ours. It inspired us to utilise the non-uniqueness of these expansions and produce a better approximation.

REFERENCES

Aurégan, Y. & Leroux, M. 2008 Experimental evidence of an instability over an impedance wall in a duct flow. *J. Sound Vib.* **317**, 432–439.

Aurégan, Y., Leroux, M. & Pagneux, V. 2005 Abnormal behavior of an acoustical liner with flow. In *Forum Acusticum, Budapest*.

Bauer, A. B. & Chapkis, R. L. 1977 Noise generated by boundary-layer interaction with perforated acoustic liners. *J. Aircraft* **14** (2), 157–160.

Bers, A. 1983 Space–time evolution of plasma instabilities: absolute and convective. In *Handbook of Plasma Physics, vol. 1: Basic Plasma Physics* (ed. A. A. Galeev & R. N. Sudan), chap. 3.2, pp. 451–517. North Holland.

Brambley, E. J. 2008 Models for acoustically-lined turbofan ducts. In *14th AIAA/CEAS Aeroacoustics Conference, 5–7 May 2008, The Westin Bayshore Vancouver, Vancouver, Canada. AIAA* 2008-2879.

Brambley, E. J. 2009 Fundamental problems with the model of uniform flow over acoustic linings. *J. Sound Vib.* **322**, 1026–1037.

Brambley, E. J. 2010 A well-posed modified Myers boundary condition. In *16th AIAA/CEAS Aeroacoustics Conference, 7–9 June 2010, Stockholm, Sweden. AIAA* 2010-3942.

Brambley, E. J. & Peake, N. 2006 Surface-waves, stability, and scattering for a lined duct with flow. In *12th AIAA/CEAS Aeroacoustics Conference, 8–10 May 2006, Cambridge, MA. AIAA*-2006-2688.

Brambley, E. J. & Peake, N. 2008 Stability and acoustic scattering in a cylindrical thin shell containing compressible mean flow. *J. Fluid Mech.* **602**, 403–426.

Brandes, M. & Ronneberger, D. 1995 Sound amplification in flow ducts lined with a periodic sequence of resonators. In *1st AIAA/CEAS Aeroacoustics Conference, 12–15 June 1995, Munich, Germany. AIAA*-95-126.

Briggs, R. J. 1964 Electron–stream interaction with plasmas. *Monograph* no. 29. MIT Press.

Campos, L. M. B. C., Oliveira, J. M. G. S. & Kobayashi, M. H. 1999 On sound propagation in a linear shear flow. *J. Sound Vib.* **219** (5), 739–770.

Chevaugeon, N., Remacle, J.-F. & Gallez, X. 2006 Discontinuous Galerkin implementation of the extended Helmholtz resonator impedance model in time domain. In *12th AIAA/CEAS Aeroacoustics Conference, 8–10 May 2006, Cambridge, MA. AIAA*-2006-2569.

Drazin, P. G. & Reid, W. H. 2004 *Hydrodynamic Stability*, 2nd edn. Cambridge University Press.

Eversman, W. & Beckemeyer, R. J. 1972 Transmission of sound in ducts with thin shear layers: convergence to the uniform flow case. *J. Acoust. Soc. Am.* **52** (1), 216–220.

Hubbard, H. H. 1995 *Aeroacoustics of Flight Vehicles: Theory and Practice, vol. 2: Noise Control*. Acoustical Society of America.

Huerre, P. & Monkewitz, P. A. 1985 Absolute and convective instabilities in free shear layers. *J. Fluid Mech.* **159**, 151–168.

Ingard, K. U. 1959 Influence of fluid motion past a plane boundary on sound reflection, absorption, and transmission. *J. Acoust. Soc. Am.* **31** (7), 1035–1036.

Lingwood, R. J. & Peake, N. 1999 On the causal behaviour of flow over an elastic wall. *J. Fluid Mech.* **396**, 319–344.

Marx, D., Aurégan, Y., Baillet, H. & Valière, J. 2010 Evidence of hydrodynamic instability over a liner in a duct with flow. *J. Sound Vib.* **329**, 3798–3812.

Michalke, A. 1965 On spatially growing disturbances in an inviscid shear layer. *J. Fluid Mech.* **23** (3), 521–544.

Michalke, A. 1984 Survey on jet instability theory. *Prog. Aerosp. Sci.* **21**, 159–199.

Myers, M. K. 1980 On the acoustic boundary condition in the presence of flow. *J. Sound Vib.* **71** (3), 429–434.

Peake, N. 1997 On the behaviour of a fluid-loaded cylindrical shell with mean flow. *J. Fluid Mech.* **338**, 387–410.

Peake, N. 2002 Structural acoustics with mean flow. In *Sound-Flow Interactions* (ed. Y. Aurégan, A. Maurel, V. Pagneux & J.-F. Pinton), pp. 248–264. Springer.

Pridmore-Brown, D. C. 1958 Sound propagation in a fluid flowing through an attenuating duct. *J. Fluid Mech.* **4**, 393–406.

Richter, C. 2009 Liner impedance modeling in the time domain with flow. PhD dissertation, Technische Universität Berlin.

Rienstra, S. W. 2003 A classification of duct modes based on surface waves. *Wave Motion* **37** (2), 119–135.

Rienstra, S. W. 2006 Impedance models in time domain, including the extended Helmholtz resonator model. In *12th AIAA/CEAS Aeroacoustics Conference, 8–10 May 2006, Cambridge, MA. AIAA*-2006-2686.

Rienstra, S. W. 2007 Acoustic scattering at a hard–soft lining transition in a flow duct. *J. Engng Maths* **59** (4), 451–475.

Rienstra, S. W. & Darau, M. 2010 Mean flow boundary layer effects of hydrodynamic instability of impedance wall. In *Proc. IUTAM Symp. on Computational Aero-Acoustics for Aircraft Noise Prediction, Southampton.*

Rienstra, S. W. & Tester, B. T. 2008 An analytic Green's function for a lined circular duct containing uniform mean flow. *J. Sound Vib.* **317**, 994–1016.

Rienstra, S. W. & Vilenski, G. G. 2008 Spatial instability of boundary layer along impedance wall. In *14th AIAA/CEAS Aeroacoustics Conference, 5–7 May 2008, The Westin Bayshore Vancouver, Vancouver, Canada. AIAA*-2008-2932.

Tester, B. J. 1973*a* The propagation and attenuation of sound in ducts containing uniform or 'plug' flow. *J. Sound Vib.* **28** (2), 151–203.

Tester, B. J. 1973*b* Some aspects of 'sound' attenuation in lined ducts containing inviscid mean flows with boundary layers. *J. Sound Vib.* **28** (2), 217–245.